

Article

Surface Functionalization of Calcium Phosphate Nanoparticles via Click Chemistry: Covalent Attachment of Proteins and Ultrasmall Gold Nanoparticles

Kathrin Kostka  and Matthias Epple * 

Inorganic Chemistry and Center for Nanointegration Duisburg-Essen (CENIDE), University of Duisburg-Essen, Universitaetsstr. 5-7, 45141 Essen, Germany; kathrin.kostka@uni-due.de

* Correspondence: matthias.epple@uni-due.de

Abstract: Calcium phosphate nanoparticles (60 nm) were stabilized with either polyethyleneimine (PEI; polycationic electrolyte) or carboxymethylcellulose (CMC; polyanionic electrolyte). Next, a silica shell was added and terminated with either azide or alkyne groups via siloxane coupling chemistry. The particles were covalently functionalized by copper-catalyzed azide-alkyne cycloaddition (CuAAC; click chemistry) with proteins or gold nanoparticles that carried the complementary group, i.e., either alkyne or azide. The model proteins hemoglobin and bovine serum albumin (BSA) were attached as well as ultrasmall gold nanoparticles (2 nm). The number of protein molecules and gold nanoparticles attached to each calcium phosphate nanoparticle was quantitatively determined by extensive fluorescent labelling and UV-Vis spectroscopy on positively (PEI) or negatively (CMC) charged calcium phosphate nanoparticles, respectively. Depending on the cargo and the nanoparticle charge, this number was in the range of several hundreds to thousands. The functionalized calcium phosphate particles were well dispersible in water as shown by dynamic light scattering and internally amorphous as shown by X-ray powder diffraction. They were easily taken up by HeLa cells and not cytotoxic. This demonstrates that the covalent surface functionalization of calcium phosphate nanoparticles is a versatile method to create transporters with firmly attached cargo molecules into cells.

Keywords: calcium phosphate; nanoparticles; surface functionalization; proteins; drug delivery; click chemistry; gold



Citation: Kostka, K.; Epple, M. Surface Functionalization of Calcium Phosphate Nanoparticles via Click Chemistry: Covalent Attachment of Proteins and Ultrasmall Gold Nanoparticles. *Chemistry* **2023**, *5*, 1060–1076. <https://doi.org/10.3390/chemistry5020072>

Academic Editors: Sofia Lima, Christoph Janiak, Sascha Rohn and Georg Manolikakes

Received: 31 March 2023

Revised: 29 April 2023

Accepted: 5 May 2023

Published: 7 May 2023



Copyright: © 2023 by the authors. Licensee MDPI, Basel, Switzerland. This article is an open access article distributed under the terms and conditions of the Creative Commons Attribution (CC BY) license (<https://creativecommons.org/licenses/by/4.0/>).

1. Introduction

Nanoparticles are widely used in many areas, as not only their size but also their shape and surface functionalization can be varied. Due to their small size, they are easily taken up by cells [1,2]. Therefore, multifunctional nanoparticles find many interesting applications as drug carriers in modern biomedicine, also with an appropriate surface functionalization to target cells or tissues [3–7]. As adsorption leads only to a weak bond between a nanoparticle and its cargo, a covalent attachment is preferable as it creates a more stable attachment [8,9]. Calcium phosphate nanoparticles are especially promising drug carriers in biomedicine [10–13] due to their high similarity to human hard tissues (bones and teeth). These are both rich in hydroxyapatite, $\text{Ca}_5(\text{PO}_4)_3\text{OH}$, the most common calcium phosphate mineral [14,15]. To ensure their colloidal stability, also in salt- and protein-containing biological media, calcium phosphate nanoparticles are usually surface-coated with polymers or polyelectrolytes. After subsequent coating with a silica shell [16–19], they can be equipped with thiol, azide or alkyne groups via siloxane chemistry. This permits a covalent attachment of molecules to their surface.

Here, we report a fundamental study where two model proteins (hemoglobin and bovine serum albumin; BSA) functionalized with alkyne groups were attached to the azide-terminated surface of calcium phosphate nanoparticles. Proteins represent important cargo

molecules which often cannot penetrate the cell membrane on their own [20]. Thus, we chose hemoglobin and BSA to serve as models for other, more functional proteins. These particles can also serve as models for nanoparticles with a protein corona, although were not designed for that purpose. As abundant plasma protein, albumin plays a prominent role in protein coronas which determine the pathway of nanoparticles in the body [21,22].

In addition, we demonstrate how azide-terminated ultrasmall gold nanoparticles can be covalently attached to alkyne-terminated calcium phosphate nanoparticles. The surface conjugation was performed by copper-catalyzed azide-alkyne cycloaddition (CuAAC; click chemistry) [23–27]. By extensive fluorescent labelling of all components, it was possible to confirm the integrity and to elucidate the chemical composition of these nanocarriers. The charge of the nanoparticles was adjusted to either positive (by polyethyleneimine; PEI) or negative (by carboxymethylcellulose; CMC). Furthermore, their cytocompatibility and their ability to cross the cell membrane were demonstrated in HeLa cell culture.

2. Materials and Methods

2.1. Reagents

The following reagents were used: albumin bovine fraction V (BSA, Serva, Heidelberg, Germany, $M_W = 66.5$ kDa); AlexaFluor[®]-647-succinimidyl ester (Invitrogen, Life Technologies, Carlsbad, CA, USA); AlexaFluor[®]-488-azide (Jena Bioscience, Jena, Germany, 95%); AlexaFluor[®]-647-alkyne (Jena Bioscience); AlexaFluor[®]-568-phalloidin (Invitrogen); aminoguanine (Alfa Aesar, Haverhill, MA, USA); aqueous ammonia solution (Carl Roth, Karlsruhe, Germany, 7.8%); (3-azidopropyl)triethoxysilane (SelectLab Chemicals, Münster, Germany, 97%); calcium lactate (Merck, Darmstadt, Germany); carboxymethylcellulose (CMC, Sigma-Aldrich, St. Louis, MO, USA, branched, $M_W = 70$ kDa); copper sulfate (CuSO_4 , Sigma-Aldrich, p.a.); diammonium hydrogen phosphate (Merck, p.a.); 3-(4,5-dimethylthiazol-2-yl)-2,5-diphenyltetrazolium bromide (MTT, Sigma-Aldrich); D-(+)-trehalose dihydrate (Sigma-Aldrich, p.a.); Dulbecco's modified Eagle's medium (DMEM, Gibco, ThermoFisher Scientific, Waltham, MA, USA); Dulbecco's phosphate buffered saline (DPBS, Gibco); ethanol (VWR, Darmstadt, Germany, p.a.); 3.7% formaldehyde solution (Merck, p.a.); glutathione (GSH, Sigma-Aldrich, 98%); hemoglobin (human, Sigma-Aldrich); methanol (VWR, p.a.); Hoechst-3342 dye (ThermoFisher Scientific); 3-methylsiloxy-1-propyne (AOB-Chem, Los Angeles, CA, USA, 95%); polyethyleneimine (PEI, Sigma-Aldrich, branched, $M_W = 25$ kDa); potassium carbonate (K_2CO_3 , Sigma-Aldrich, p.a.); propargyl-PEG3-aminoxy linker (Broadpharm, San Diego, CA, USA); sodium ascorbate (Sigma-Aldrich, 99%); sodium borohydride (NaBH_4 , Sigma-Aldrich, 96%); sodium hydroxide (NaOH, VWR, p.a.); tetraethylorthosilicate (TEOS, Sigma-Aldrich, 98%); tris(3-hydroxypropyl-triazolylmethyl)amine (THPTA, Sigma-Aldrich, 95%).

For all syntheses and purifications, ultrapure water (Purelab ultra instrument from ELGA, Celle, Germany) was used. All syntheses and analyses were carried out in water unless otherwise noted.

2.2. Instruments

All calcium phosphate nanoparticles described in the following syntheses were isolated and purified by centrifugation with a 5430/5430 R Centrifuge (Eppendorf AG, Hamburg, Germany) at room temperature for 30 min at 14,200 rpm in 5 mL tubes. The gold nanoparticles were purified for 40 min at 4000 rpm in centrifugal spin filters (Amicon[®] Ultra, 3 kDa MWCO, Merck). The particles were washed with water and redispersed with a sonotrode (UP50H, Sonotrode N7, amplitude 70%, pulse duration 0.12 s, Hielscher Ultrasonics GmbH, Teltow, Germany). To determine the calcium concentration in the dispersions, atomic absorption spectroscopy (AAS) with an M-Series AA spectrometer (ThermoElectron Corporation, Waltham, MA, USA) was performed. For this, 0.5 mL of the dispersion was mixed with 0.5 mL HCl (0.1 M) and filled up to 5 mL with water. To determine the gold concentration, 20 μL of the gold-containing sample was reacted with 980 μL aqua regia and filled up to 5 mL with water for the AAS measurements.

After characterization and for storage, the particles were lyophilized in a D-(+)-trehalose solution (20 mg mL⁻¹; cryoprotectant) with a Christ Alpha 2-4 LSC instrument (Martin Christ GmbH, Osterode am Harz, Germany). For subsequent investigations, the nanoparticles were redispersed in water.

Dynamic light scattering (DLS) for particle size determination (number distribution) and zeta potential measurement was performed with 760 µL of the nanoparticle dispersion in a dip cell kit (Malvern, UK) in a Zetasizer Nano ZS instrument ($\lambda = 633$ nm, Malvern Nano ZS ZEN 3600 (Malvern Panalytical; Malvern, UK). For scanning electron microscopy (SEM), 5 µL of the dispersion was placed on a sample holder, dried in air, sputtered with gold/palladium, and examined with an Apreo S LoVac microscope (ThermoFisher Scientific). Energy-dispersive X-ray spectroscopy (EDX; detector type: SUTW-Sapphire) was used together with the SEM. The samples were analyzed by EDX without prior sputtering. The average particle diameter was calculated from visual inspection of at least 50 nanoparticles in SEM images with the software ImageJ [28].

X-ray powder diffraction (XRD) was performed with Cu K α radiation ($\lambda = 1.54$ Å) on silicon single crystal sample holders cut along (911) with a Bruker D8 instrument (Bruker, Billerica, MA, USA). A range of 5–90 °2 θ , a step size of 0.01 °2 θ , a counting time of 0.6 s, and a nickel filter were used.

UV–Vis spectroscopy in a 400 µL Suprasil[®] quartz cuvette was carried out with a Varian Cary 300 Bio spectrophotometer (Agilent Technologies, Santa Clara, CA, USA). For fluorescence spectroscopy, the particles were dispersed in water and measured in a quartz cuvette with an Agilent Technologies Cary Eclipse spectrophotometer. Differential centrifugal sedimentation (DCS) with a DC24000 UHR instrument (CPS Instruments, Prairieville, LA, USA) was used to determine the size of the water-dispersed ultrasmall gold nanoparticles. Prior to the measurement, a sucrose gradient was created, and a calibration was performed with a PVC calibration dispersion standard (diameter 483 nm; CPS Instruments).

2.3. Synthesis of CaP/PEI/SiO₂-N₃ and CaP/CMC/SiO₂-N₃ Nanoparticles

The synthesis of PEI- or CMC-stabilized calcium phosphate (CaP) nanoparticles was carried out as follows, following a modified procedure first reported by Rojas et al. [18]. Extending these earlier results where only cationic nanoparticles with a primary PEI shell were prepared, we have extended the synthetic procedure to prepare anionic nanoparticles with CMC as primary shell. First, a calcium lactate solution (18 mmol L⁻¹, 5 mL min⁻¹, pH 10), a diammonium hydrogen phosphate solution (10.8 mmol L⁻¹, 5 mL min⁻¹, pH 10) and either a PEI solution (2 g L⁻¹, 7 mL min⁻¹) or a CMC solution (2 g L⁻¹, 7 mL min⁻¹) were pumped for 30 s into a beaker containing 10 mL water at room temperature with two peristaltic pumps. After stirring for 20 min, the silica shell was applied. 12 mL of the CaP-PEI or CaP-CMC nanoparticle dispersion, 60 µL tetraethylorthosilicate (TEOS), 120 µL ammonia solution (7.8%) and 48 mL ethanol were rapidly mixed under stirring. The dispersion was stirred for 16 h. The particles were purified by centrifugation and redispersed in 12 mL of water to obtain CaP/PEI/SiO₂ and CaP/CMC/SiO₂ nanoparticles.

For the attachment of azide groups to the particle surface, 12 mL of the redispersed CaP/PEI/SiO₂ or CaP/CMC/SiO₂ particles were mixed with 48 mL ethanol, 58.8 µL ammonia solution (7.8%), and 181 µL (3-azidopropyl)triethoxysilane and stirred for 6 h. The resulting CaP/PEI/SiO₂-N₃ and CaP/CMC/SiO₂-N₃ nanoparticles were purified by centrifugation.

2.4. Synthesis of CaP/PEI/SiO₂-Alkyne and CaP/CMC/SiO₂-Alkyne Nanoparticles

For the attachment of alkyne groups on the particle surface, the same procedure as in 2.3 was followed, except for the use of 3-trimethylsiloxy-1-propyne instead of (3-azidopropyl)triethoxysilane.

2.5. Synthesis of Fluorescent and Alkyne-Conjugated BSA and Hemoglobin

First, BSA and hemoglobin (Hem) (1 mg mL^{-1}) were conjugated with AF647-succinimidyl ester according to the manufacturer's instructions. Centrifugal spin filters were used for three times purification (Amicon® Ultra, 3 kDa MWCO) at 4000 rpm for 40 min. The labelling allowed to quantify Hem-AF647 and BSA-AF647 in subsequent synthesis steps by UV spectroscopy after recording calibration curves as the protein concentration was known (1 mg mL^{-1}).

Next, the fluorescent proteins were conjugated with alkyne groups. To attach alkyne groups to BSA-AF647 and Hem-AF647, the fluorescently labelled proteins (1 mg mL^{-1}) were incubated with $125 \text{ }\mu\text{M}$ propargyl-PEG3-aminoxy linker for 12 h at $37 \text{ }^\circ\text{C}$ under stirring. Subsequently, BSA-AF647-alkyne and Hem-AF647-alkyne were purified twice with centrifugal spin filters (3 kDa MWCO) at 4000 rpm for 40 min to remove excess linker and redispersed in water.

2.6. Conjugation of BSA-AF647-Alkyne and Hem-AF647-Alkyne to CaP/PEI/SiO₂-N₃ and CaP/CMC/SiO₂-N₃ Nanoparticles

BSA-AF647-alkyne and Hem-AF647-alkyne were coupled to CaP/PEI/SiO₂-N₃ and CaP/CMC/SiO₂-N₃ nanoparticles by CuAAC, respectively. For this, 0.5 mL of CaP/PEI/SiO₂-N₃ or CaP/CMC/SiO₂-N₃ nanoparticle dispersion were used: 95 mg mL^{-1} CaP/PEI/SiO₂-N₃ and 93 mg mL^{-1} CaP/CMC/SiO₂-N₃ for the conjugation with BSA-AF647-alkyne; 58 mg mL^{-1} CaP/PEI/SiO₂-N₃ and 56 mg mL^{-1} CaP/CMC/SiO₂-N₃ for the conjugation with Hem-AF647-alkyne, respectively. Each dispersion was mixed with $0.35 \text{ }\mu\text{L}$ NaOH (0.1 M), $38.5 \text{ }\mu\text{L}$ aminoguanidine (1 mg mL^{-1}), $36.5 \text{ }\mu\text{L}$ sodium ascorbate (100 mM), $3.65 \text{ }\mu\text{L}$ of a solution containing CuSO₄ ($40 \text{ }\mu\text{M}$) and THPTA ($200 \text{ }\mu\text{M}$), and $25 \text{ }\mu\text{L}$ of BSA-AF647-alkyne (1 mg mL^{-1}) or $25 \text{ }\mu\text{L}$ of Hem-AF647-alkyne (1 mg mL^{-1}). Each dispersion was stirred for 1 h at room temperature under light exclusion. The particles were purified by spin filtration and redispersed in 0.5 mL water by ultrasonication for 4 s.

2.7. Conjugation of AF488-N₃ to CaP/PEI/SiO₂-Alkyne and CaP/CMC/SiO₂-Alkyne Nanoparticles

For the click reaction of AF488-N₃ to CaP/PEI/SiO₂-alkyne and CaP/CMC/SiO₂-alkyne nanoparticles, 5 mL of the nanoparticle dispersion was mixed with $167 \text{ }\mu\text{L}$ AF488-N₃, $385 \text{ }\mu\text{L}$ aminoguanidine (1 mg mL^{-1}), $3.5 \text{ }\mu\text{L}$ NaOH (0.1 M), $36.5 \text{ }\mu\text{L}$ of a solution containing CuSO₄ ($40 \text{ }\mu\text{M}$) and THPTA ($200 \text{ }\mu\text{M}$), and $365 \text{ }\mu\text{L}$ sodium ascorbate (100 mM) and stirred for 1 h at RT under light exclusion. The amount of AF488-N₃ was set to leave some alkyne groups on the calcium phosphate nanoparticles unconjugated. The particles were purified by spin filtration and redispersed in 5 mL water by ultrasonication for 4 s.

2.8. Synthesis of Fluorescent Ultrasmall Gold Nanoparticles (2 nm; Au-AF647-N₃)

Ultrasmall gold nanoparticles carrying AF647 were prepared as described earlier by clicking AF647-alkyne to the surface of azide-functionalized glutathione-coated gold nanoparticles [29]. In order to load the surface of the Au-GSH-N₃ nanoparticles with fluorescent AF647-alkyne molecules, but to leave some azide groups free for subsequent coupling, only 1/3 of AF647-alkyne of the synthesis protocol reported in [29] was used. The particles had a diameter of the gold core of 2 nm and were characterized by UV spectroscopy, fluorescence spectroscopy, atomic absorption spectroscopy, NMR spectroscopy, and differential centrifugal sedimentation, giving the same results as in the standard synthesis reported in [29].

2.9. Conjugation of Ultrasmall Au-AF647-N₃ Nanoparticles to CaP/PEI/SiO₂-AF488-Alkyne or CaP/CMC/SiO₂-AF488-Alkyne Nanoparticles

$50 \text{ }\mu\text{L}$ of Au-AF647-N₃ nanoparticle dispersion (1 mg mL^{-1}) was used for conjugation to CaP/PEI/SiO₂-AF488-alkyne and CaP/CMC/SiO₂-AF488-alkyne nanoparticles, respectively. CuAAC was carried out under the same conditions as during the clicking of the alkyne-terminated proteins to the azide-terminated calcium phosphate nanoparticles

described above, leading to CaP/PEI/SiO₂-AF488-Au-AF647 and CaP/CMC/SiO₂-AF488-Au-AF647 nanoparticles. The particles were purified by spin filtration and redispersed in 0.5 mL water by ultrasonication for 4 s.

2.10. Cell Culture Studies

HeLa cells were cultured at 37 °C in 5% CO₂ atmosphere in cell culture flasks and then seeded onto the well plates for microscopy. Dulbecco's modified Eagle's medium (DMEM) with 10% fetal bovine serum, 100 U mL⁻¹ penicillin, and 100 U mL⁻¹ streptomycin served as cell culture medium.

An MTT assay was performed by spectrophotometric analysis. HeLa cells were transferred into a 24-well plate with 5×10^4 cells/well in 500 µL DMEM and cultivated for 24 h. 30 µL (1 mg mL⁻¹) of the different nanoparticle dispersions was added, respectively, for incubation for 24 h. Subsequently, the cells were washed three times with 500 µL DPBS, treated with 300 µL 3-(4,5-dimethylthiazol-2-yl)-2,5-diphenyltetrazolium bromide (MTT, 1 mg mL⁻¹) and incubated for 1 h at 37 °C. Then, the MTT solution was removed and replaced with 300 µL DMSO for 30 min. Finally, 100 µL of the DMSO solution was put into a 96-well plate for spectrophotometric analysis at 570 nm with a multiscan FC instrument (Thermo Fisher Scientific). The relative cell viability was normalized to the control group (mock), i.e., untreated cells.

For nanoparticle uptake, HeLa cells (5×10^4 cells/well) were cultured in an 8-well plate in 250 µL of DMEM for 24 h prior to incubation with the nanoparticles. Subsequently, 30 µL of the nanoparticle dispersion (1 mg mL⁻¹) diluted with 220 µL of DMEM was added. The incubation time was 24 h. Then, the cells were washed twice with DPBS to remove dead cells and free nanoparticles. For cell fixation, 150 µL of a 3.7% formaldehyde solution was added for 15 min at room temperature. The fixed cells were incubated with AF568-phalloidin (30 µL in 2 mL DPBS; 230 µL/well) for 20 min for actin staining. For nuclear staining, a Hoechst-3342 solution (4 µL in 2 mL DPBS; 230 µL/well) was applied for 15 min. The cells were washed twice with DPBS after each fixation and staining step. Images were taken with a fluorescence microscope (Keyence Bioevo BZ-9000, Neu-Isenburg, Germany) with a TRITC filter (Ex. 540/25 nm, DM 565 nm, BA 605/55 nm) and a FITC filter (Ex. 470/40 nm, DM 495 nm, BA 535/50 nm). A confocal laser scanning microscope (Leica TCS SP8X FALCON, Wetzlar, Germany) with laser wavelengths of 405 nm (nuclear staining; Hoechst-3342), 488 nm (AF488), 568 nm (AlexaFluor568 phalloidin), 647 nm (AF647), and a pulsed laser WLL (470–670 nm) was used for higher resolution, together with an HC PL APO UVIS CS2 63X/1.2 water immersion lens.

3. Results and Discussion

The calcium phosphate nanoparticles were prepared with either positive charge (by PEI) or negative charge (by CMC) to elucidate the effect of the particle charge on the biomolecule attachment and the subsequent particle effect on cells. A shell of silica to permit a covalent surface functionalization by azide or alkyne groups was added. Copper-catalyzed azide-alkyne cycloaddition (CuAAC; click chemistry) was used for subsequent covalent attachment of molecules and gold nanoparticles [30]. For this, BSA-AF647 and Hem-AF647 proteins were previously conjugated with alkyne groups, and ultrasmall gold nanoparticles were functionalized with azide groups. In the following, we denote the particles in abbreviated form, indicating the particle charge and omitting the omnipresent silica shell. Thus, the particle type CaP/CMC/SiO₂-AF488 is abbreviated as CaP^{neg}-AF488, the particle type CaP/PEI/SiO₂-BSA is abbreviated as CaP^{pos}-BSA, etc. Figure 1 shows all steps of the particle synthesis.

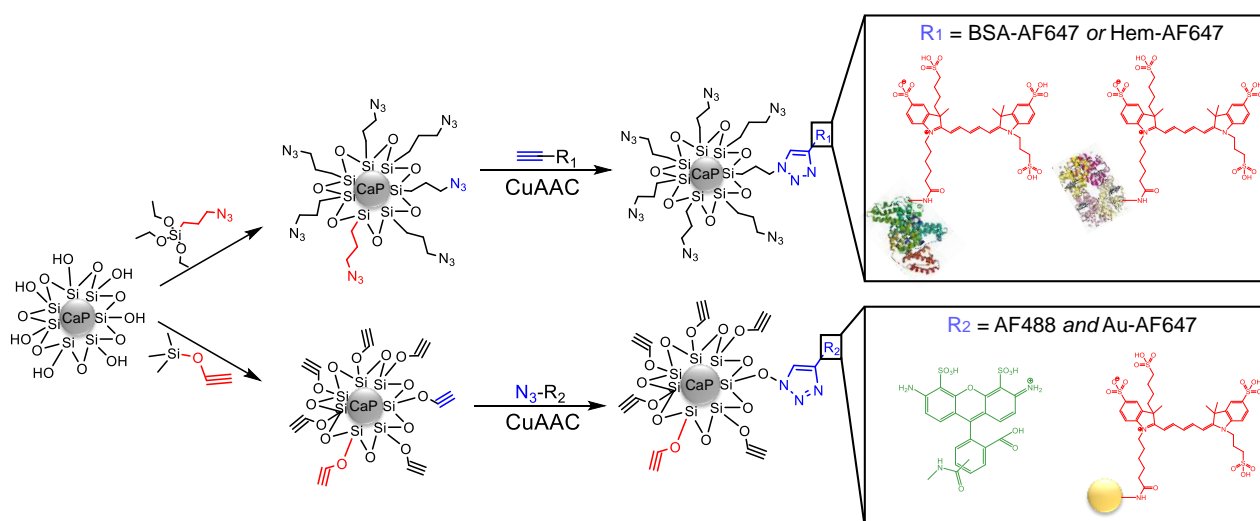


Figure 1. Steps of the surface functionalization of calcium phosphate nanoparticles (CaP) with Hem-AF647-, BSA-AF647-, and AF647-labelled ultrasmall gold nanoparticles (Au-AF647).

The attachment of fluorescently labelled bovine serum albumin (BSA-AF647) led to CaP^{pos} -BSA-AF647 and CaP^{neg} -BSA-AF647 nanoparticles, and the attachment of fluorescently labelled hemoglobin (Hem-AF647) led to CaP^{pos} -Hem-AF647 and CaP^{neg} -Hem-AF647 nanoparticles. Each BSA molecule carried 3.6 AF647 molecules, and each hemoglobin molecule carried 3.0 AF647 molecules. These labelling degrees were later used to compute the number of protein molecules on each calcium phosphate nanoparticle.

We also attached AF647-carrying ultrasmall gold nanoparticles (Au-AF647) together with the dye AF488, leading to CaP^{pos} -AF488-Au-AF647 and CaP^{neg} -AF488-Au-AF647 nanoparticles. As fluorescent control particles without cargo, CaP^{pos} -AF488 and CaP^{neg} -AF488 nanoparticles were prepared. All particles were thoroughly purified and characterized. Figure 2 schematically shows the synthetic pathways to all prepared nanoparticles.

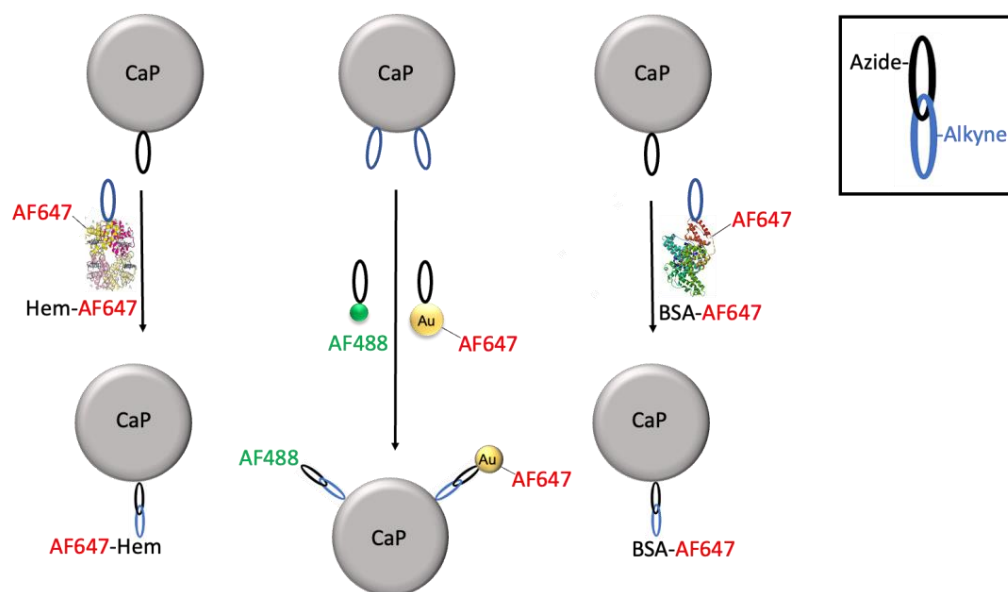


Figure 2. Summary of the surface conjugation of Hem-AF647-, BSA-AF647-, and AF647-carrying ultrasmall gold nanoparticles to calcium phosphate nanoparticles. All conjugated moieties were fluorescently labelled for detection and quantification.

The composition of the particles was quantitatively determined by UV–Vis spectroscopy (Figure 3). The recording of calibration curves and the determination of the calcium concentration in the dispersion by AAS permitted to compute the number of molecules attached to each nanoparticle (see below).

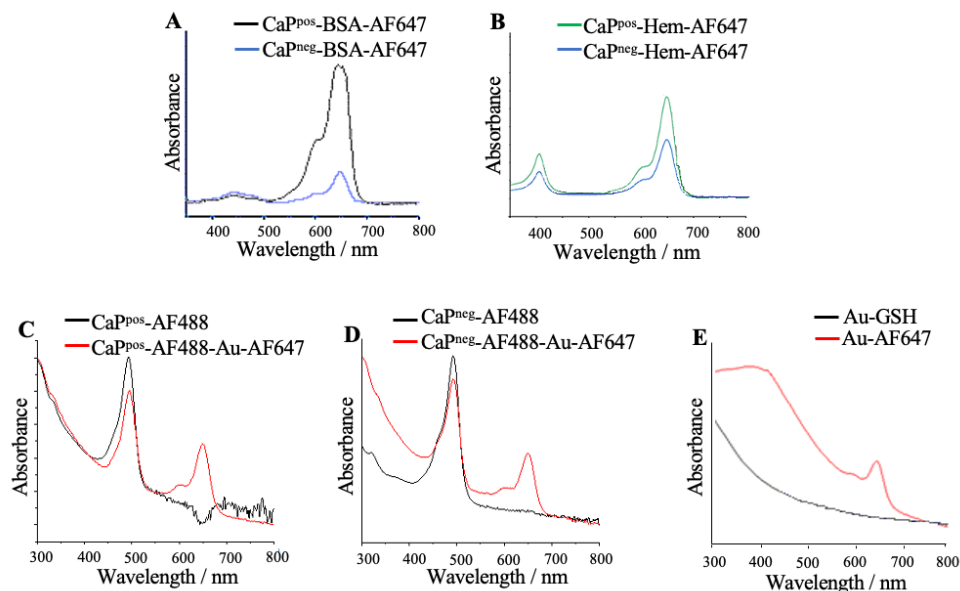


Figure 3. UV–Vis spectra of the functionalized calcium phosphate nanoparticles (A–D) and of ultra-small gold nanoparticles before (Au-GSH; GSH = glutathione) and after (Au-AF647) the attachment of AF647 (E). All fluorescent labels were clearly detectable in the UV spectra and later used to quantify the individual species. Note the absorption of the protein hemoglobin itself at approximately 400 nm in (B).

All particles showed the strong fluorescence of the attached molecules (Figure 4). The green color depicts the presence of AF488 and the red color the presence of AF647. In general, the particle charge does not play a significant role for the optical properties and also does not affect the conjugation.

The solid core diameter of the particles was determined by scanning electron microscopy (SEM). All calcium phosphate nanoparticles had an approximately spherical (or globular) shape (Figure 5). The particle size varied between 39 nm and 90 nm, depending on the synthesis, but did not depend on the particle charge (see also Table 1). The calcium phosphate nanoparticles were agglomerated to some degree in the SEM due to the drying process. For the particle size distribution, we used the particle diameter that a spherical particle would have (by visual inspection). The gold nanoparticles were too small (2 nm) to be detectable by SEM.

Dynamic light scattering (DLS) was performed to determine the hydrodynamic diameter and the water dispersibility of the nanoparticles. The increasing hydrodynamic diameter confirmed the successful attachment of the fluorescent molecules and of gold nanoparticles (Figure 6). The hydrodynamic diameter was between 129 nm and 340 nm, i.e., always larger than the solid core diameter as determined by SEM, indicating a moderate agglomeration in dispersion. In general, the gold nanoparticles were too small for DLS [29]; therefore, they were characterized by differential centrifugal sedimentation (DCS).

To determine the elemental composition of the functionalized nanoparticles, energy-dispersive X-ray spectroscopy (EDX) was performed. All expected elements were found (Figure 7). An EDX mapping of similar silica-coated calcium phosphate nanoparticles was reported in [16], showing a homogeneous distribution of calcium, phosphate, and silicon.

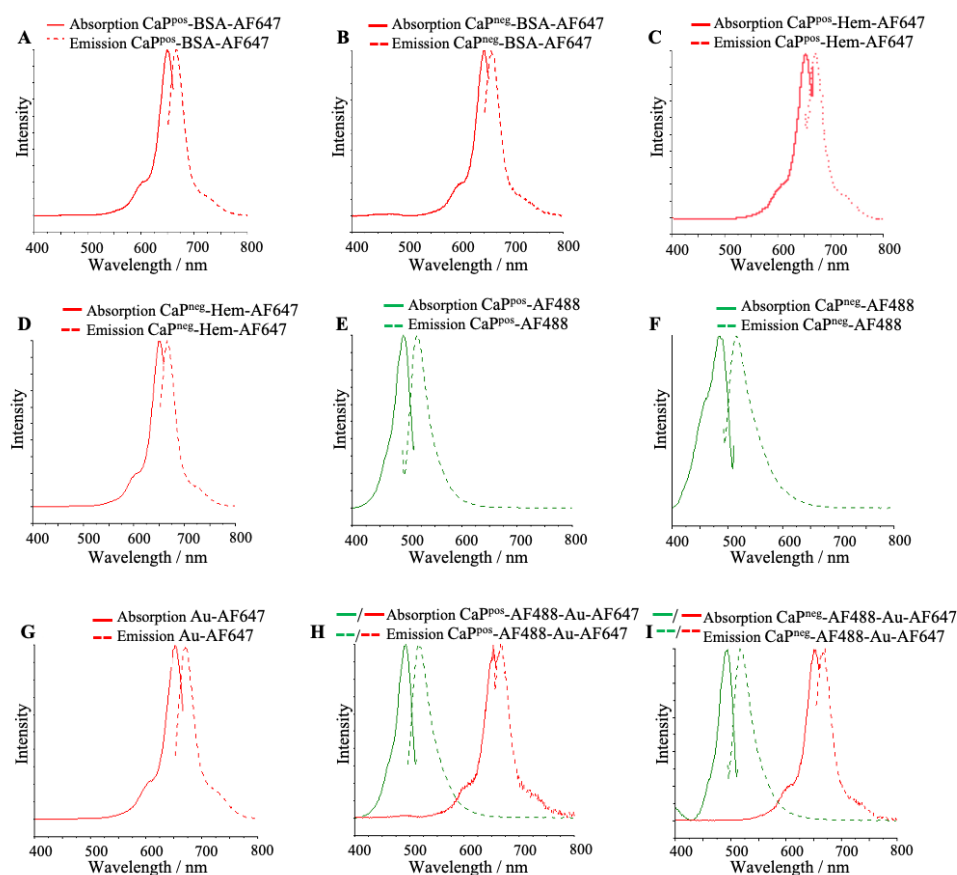


Figure 4. Absorption and emission spectra of functionalized calcium phosphate nanoparticles (A–F) and of ultrasmall gold nanoparticles before (G) and after attachment to calcium phosphate (H,I). In all cases, the expected fluorescence signals were present, giving a green (AF488) or a red (AF647) fluorescence.

X-ray powder diffraction was carried out to determine the internal crystallinity of the nanoparticles (Figure 8). The nanoparticles were almost X-ray amorphous (extreme broadening of the peaks) and did not show the characteristic peaks of the most prominent calcium phosphate phase, i.e., hydroxyapatite. According to our experience and the literature, it is likely that they consist of X-ray amorphous calcium phosphate with a stoichiometry close to hydroxyapatite [31–33].

From the calcium concentration in a given dispersion by AAS and the solid core diameter by SEM, the particle concentration can be computed if uniform spherical particles are assumed. Here, the solid core diameters of the nanoparticles with the same stabilization (PEI or CMC) were averaged/normalized for both syntheses and used for the calculations. The concentration of calcium in the samples was converted into the concentration of stoichiometric hydroxyapatite, $\text{Ca}_5(\text{PO}_4)_3\text{OH}$, and then into a volume by the density of hydroxyapatite (3140 kg m^{-3}). The combination of the calcium concentration (giving the total particle volume) and the average particle diameter (giving the volume of one particle) gave the concentration of calcium phosphate nanoparticles (see [18] for details of the computation). All particles had the expected zeta potential, i.e., the cationic polyelectrolyte PEI and the anionic polyelectrolyte CMC gave the particles their characteristic charge. The attachment of the cargo did not reverse the particle charge, i.e., cationic nanoparticles remained positively charged and anionic nanoparticles remained negatively charged. This led to well-dispersed particles as indicated by the hydrodynamic diameter as determined by DLS, despite some agglomeration as the comparison with the solid core diameter by SEM shows. Table 1 summarizes the characterization data of all functionalized calcium phosphate nanoparticles.

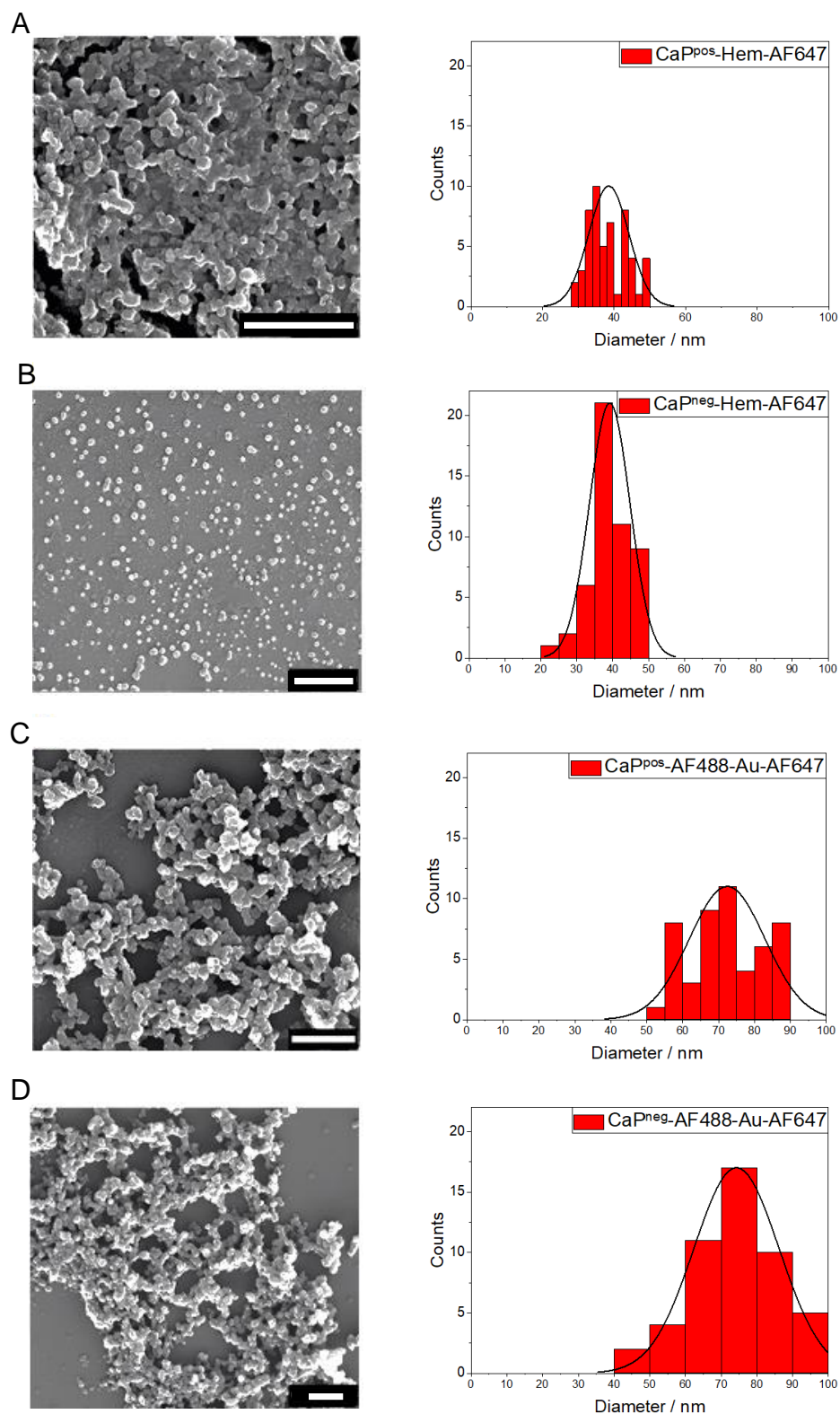
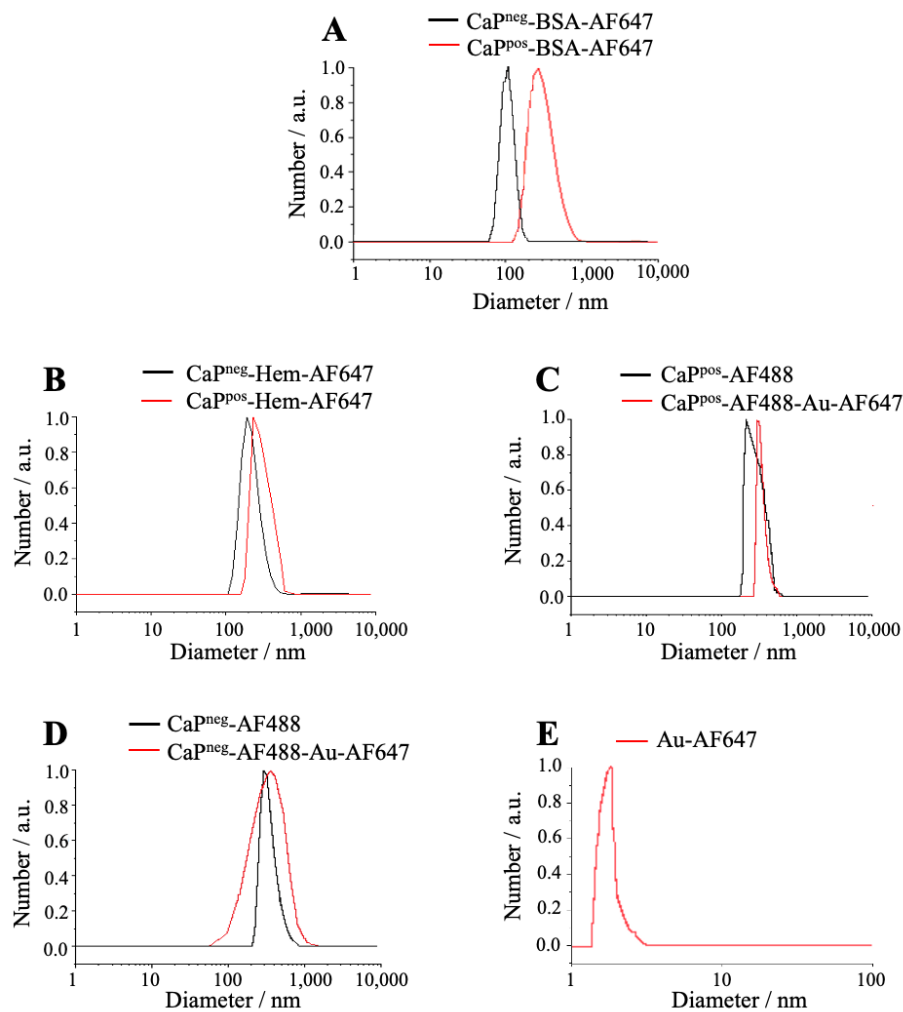


Figure 5. Representative SEM images of surface-functionalized calcium phosphate nanoparticles. Scale bars 500 nm. (A) $\text{CaP}^{\text{pos}}\text{-Hem-AF647}$, (B) $\text{CaP}^{\text{neg}}\text{-Hem-AF647}$, (C) $\text{CaP}^{\text{pos}}\text{-AF488-Au-AF647}$ and (D) $\text{CaP}^{\text{neg}}\text{-AF488-Au-AF647}$ nanoparticles. The corresponding particle size distributions indicate the polydispersity of the particles, based on the assumption of spherical particles.

Table 1. Properties of PEI- and CMC-stabilized calcium phosphate nanoparticles with different conjugated molecules.

	CaP ^{pos} -BSA-AF647	CaP ^{neg} -BSA-AF647	CaP ^{pos} -Hem-AF647	CaP ^{neg} -Hem-AF647	CaP ^{pos} -AF488	CaP ^{neg} -AF488	CaP ^{pos} -AF488-Au-AF647	CaP ^{neg} -AF488-Au-AF647
Solid core diameter by SEM/nm	64 ± 6	49 ± 5	39 ± 6	39 ± 6	72 ± 11	74 ± 12	72 ± 11	74 ± 12
<i>w</i> (Ca ²⁺) in dispersion by AAS/kg m ⁻³	0.092	0.090	0.056	0.053	0.096	0.092	0.046	0.040
<i>w</i> (HAP) in dispersion/kg m ⁻³ (computed)	0.231	0.226	0.140	0.133	0.241	0.231	0.115	0.100
<i>N</i> (nanoparticles) in dispersion/m ⁻³ (computed)	5.35 × 10 ¹⁷	1.17 × 10 ¹⁸	1.44 × 10 ¹⁸	1.36 × 10 ¹⁸	3.92 × 10 ¹⁷	3.46 × 10 ¹⁷	1.88 × 10 ¹⁷	1.51 × 10 ¹⁷
Hydrodynamic particle diameter by DLS/nm	181 ± 9	149 ± 10	126 ± 9	206 ± 16	200 ± 8	291 ± 15	301 ± 7	340 ± 21
Polydispersity index (PDI) by DLS	0.32 ± 0.02	0.33 ± 0.01	0.29 ± 0.07	0.35 ± 0.02	0.22 ± 0.14	0.31 ± 0.02	0.29 ± 0.06	0.24 ± 0.12
Zeta potential by DLS/mV	+17 ± 2	-16 ± 1	+20 ± 4	-24 ± 6	+20 ± 1	-17 ± 1	+14 ± 1	-12 ± 6

**Figure 6.** Particle size distribution (by number) of calcium phosphate nanoparticles by dynamic light scattering (DLS) (A–D), and differential centrifugal sedimentation (DCS) of Au-AF647 nanoparticles (E).

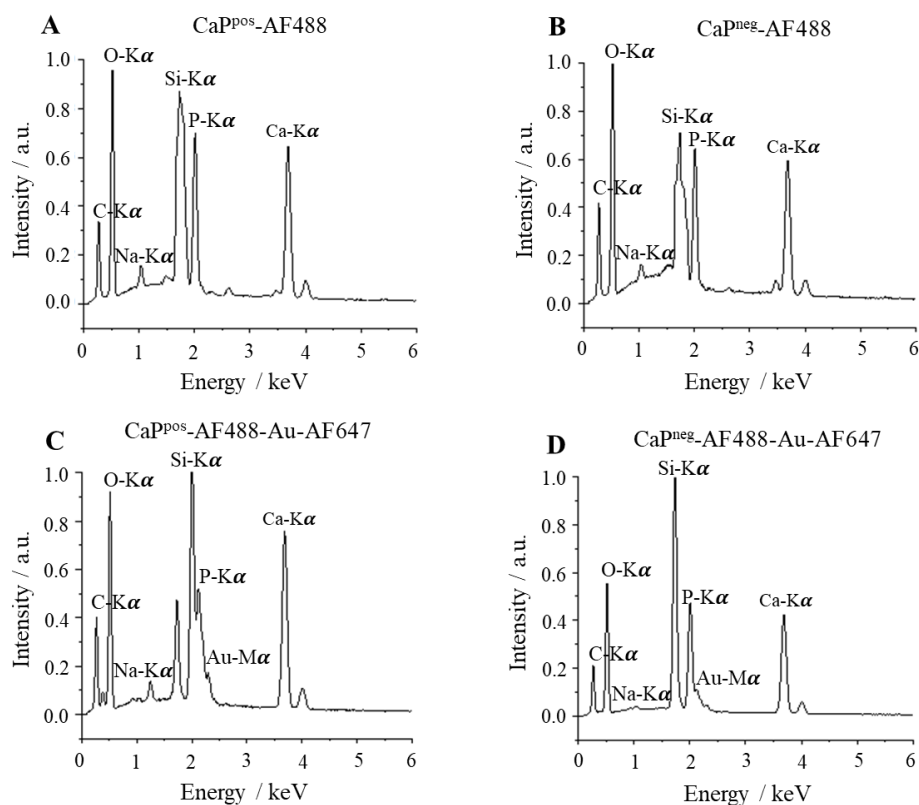


Figure 7. Representative energy-dispersive X-ray spectra (EDX) of calcium phosphate nanoparticles carrying AF488 (A,B) and AF488 together with Au-AF647 nanoparticles (C,D).

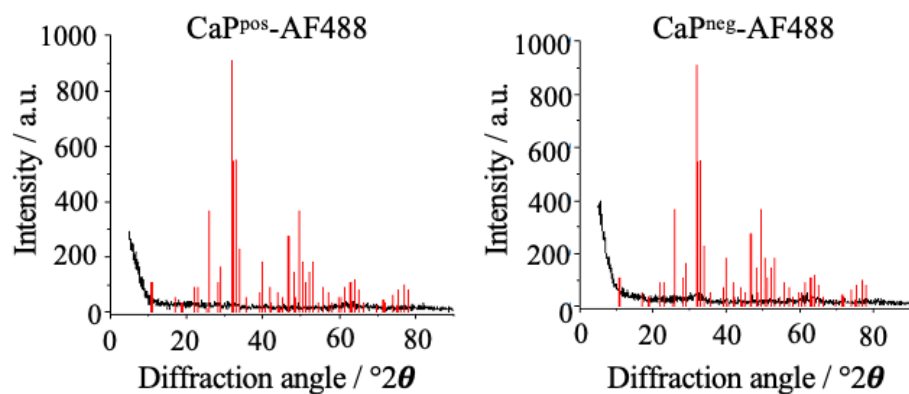


Figure 8. Representative X-ray powder diffractograms of functionalized calcium phosphate nanoparticles. The peaks of crystalline hydroxyapatite (JCPDS No. 00-009-0432) are shown for comparison as red bars.

The composition of the functionalized nanoparticles comprises the number of attached cargo molecules on each nanoparticle. This was possible by recording UV–Vis spectra of all dispersions and quantifying the absorption of each fluorophore with Lambert–Beer’s law. Previously, calibration curves were recorded for each cargo compound. The molar masses of AF647-alkyne (910 Da), BSA-AF647-alkyne (67.4 kDa), Hem-AF647-alkyne (65.9 kDa), AF488-alkyne (774 Da), AF647-azide (940 Da) and AF488-azide (659 Da), were used to convert mass concentrations into molar concentrations. The molar ratio of cargo molecules to calcium phosphate nanoparticles then gave the desired loading number.

The number of conjugated gold nanoparticles was determined in the same way. First, the concentration of gold nanoparticles in the dispersion was computed with the average gold core diameter of 2 nm that was measured earlier [29]. Each gold nanoparticle con-

tains approximately 250 gold atoms if assumed as spherical and weighs approximately $250 \times M(\text{Au})/N_A = 250 \times 197 \text{ g mol}^{-1}/6.023 \times 10^{23} \text{ mol}^{-1} = 8.2 \times 10^{-20} \text{ g}$. Again, the concentration of AF647 in the dispersion was determined by quantitative UV-Vis spectroscopy. The molar ratio of AF647 molecules and gold nanoparticles gave the number of AF647 on each gold nanoparticle with 2.3 (Table 2). The number of gold nanoparticles attached to each calcium phosphate nanoparticle then followed from the concentrations of gold and calcium in the dispersion.

Table 2. Gold concentration in dispersion and the number of AF647 molecules attached to each gold nanoparticle (Au-NP; 2 nm), measured for the functionalized calcium phosphate nanoparticles CaP^{pos}-AF488-Au-AF647 and CaP^{neg}-AF488-Au-AF647.

	$w(\text{Au})$ in Dispersion (AAS)/ kg m^{-3}	$c(\text{Au})$ in Dispersion (AAS)/ mol m^{-3}	$N(\text{Au-NP})$ in Dispersion/ m^{-3}	$c(\text{Au-NP})$ in Dispersion/ mol m^{-3}	$c(\text{AF647})$ in Dispersion/ mol m^{-3}
CaP ^{pos} -AF488-Au-AF647	4.00×10^{-2}	2.03×10^{-1}	4.95×10^{20}	8.22×10^{-4}	1.89×10^{-3}
CaP ^{neg} -AF488-Au-AF647	5.75×10^{-3}	2.92×10^{-2}	7.11×10^{19}	1.18×10^{-4}	2.71×10^{-4}

Table 3 shows the numbers of protein molecules and gold nanoparticles attached to each calcium phosphate nanoparticle. The number of attached protein molecules differed considerably between BSA and Hem. The lower number of attached BSA molecules on negatively charged calcium phosphate nanoparticles may be explained by its negative charge at the moderately alkaline pH during clicking: The isoelectric point of BSA is 4.5 to 5 [34], and that of hemoglobin is 7.1 to 7.3 [35], i.e., hemoglobin is less negatively charged than BSA at neutral pH.

Table 3. Number of cargo proteins and nanoparticles on the functionalized calcium phosphate nanoparticles as computed by calcium phosphate particle concentrations (Table 1) and conjugated molecule concentrations (by UV spectroscopy).

	CaP ^{pos} -BSA-AF647	CaP ^{neg} -BSA-AF647	CaP ^{pos} -Hem-AF647	CaP ^{neg} -Hem-AF647	CaP ^{pos} -AF488	CaP ^{neg} -AF488	CaP ^{pos} -AF488-Au-AF647	CaP ^{neg} -AF488-Au-AF647
Protein molecules on each CaP nanoparticle	385	9	127	99	-	-	-	-
Au nanoparticles on each CaP nanoparticle	-	-	-	-	-	-	2717	452
AF647 molecules on each CaP nanoparticle	1385	34	380	297	-	-	6250	1040
AF488 molecules on each CaP nanoparticle	-	-	-	-	9320	7920	1310	1210
Molar ratio Ca: Au by AAS	-	-	-	-	-	-	85:15	97:3
Molar ratio Ca: Au by EDX	-	-	-	-	-	-	93:7	95:5

For ultrasmall gold nanoparticles, the ratio of calcium to gold as determined by AAS and EDX was similar. Due to the presence of glutathione on the surface of the gold nanoparticles, they are expected to carry a negative charge as well at moderately alkaline pH. This explains why fewer gold nanoparticles are conjugated to negatively charged calcium phosphate nanoparticles. In contrast, the number of AF488 molecules clicked to calcium phosphate did not depend on the particle charge.

Of course, the numbers given in Tables 2 and 3 must be considered as being associated with a considerable uncertainty. This arises from a number of assumptions such as monodisperse and spherical nanoparticles. Furthermore, the applied analytical methods (UV-Vis, AAS) all carry some instrumental uncertainty. It is not possible to quantitatively

determine all these uncertainties, but it is realistic to assume that the cargo numbers given in Tables 2 and 3 carry an uncertainty of at least $\pm 30\%$. Nevertheless, they give at least an impression on the conjugated cargo and allow to identify trends in the conjugation efficiency.

To test the efficiency of the calcium phosphate nanoparticles to transport their cargo across the cell membrane into cells, uptake studies with HeLa cells were performed (Figure 9). All types of nanoparticles were well taken up by the cells, with a slight preference for positively charged nanoparticles. The cargo (Hem, BSA, Au-NPs) was well transported into the cells as indicated by the corresponding fluorescence signals. It has been shown earlier that many dissolved proteins alone cannot cross the cell membrane [36–39] but ultrasmall gold nanoparticles are well able to do that [40]. The co-localization of AF488 and AF647 indicates that the gold nanoparticles remained attached to the calcium phosphate nanoparticles during the uptake, i.e., that they are not separated and taken up by cells separately.

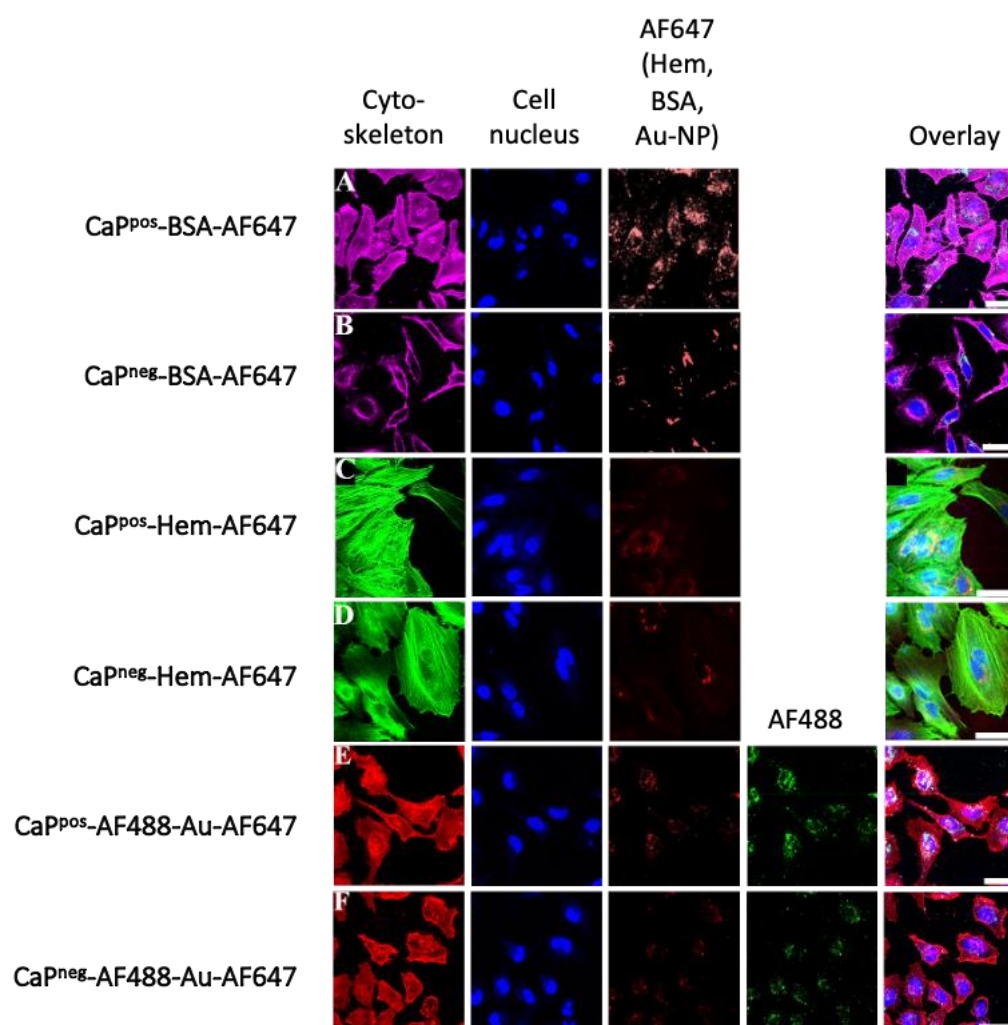


Figure 9. CLSM images demonstrate the uptake of functionalized calcium phosphate nanoparticles by HeLa cells. All particle types easily entered the cells. Actin staining with AF568-phalloidin (magenta; red) or AF488-phalloidin (green), nuclear staining with HOECHST33342 (blue). (A) CaP^{pos}-BSA-AF647, (B) CaP^{neg}-BSA-AF647, (C) CaP^{pos}-Hem-AF647, (D) CaP^{neg}-Hem-AF647, (E) CaP^{pos}-AF488-Au-AF647 and (F) CaP^{neg}-AF488-Au-AF647. Scale bars 20 μm .

Calcium phosphate nanoparticles enter eukaryotic cells via endocytosis [41] and end up in endolysosomes [36–38]. It was suggested that they will dissolve there under the acidic conditions in an endolysosome to release their cargo. It is very likely that the endolysosome

bursts due to increased osmotic pressure after the dissolution of calcium phosphate [42], thus the cargo will eventually reach the cytosol.

Finally, it was shown by an MTT assay that the functionalized calcium phosphate nanoparticles were not cytotoxic (Figure 10).

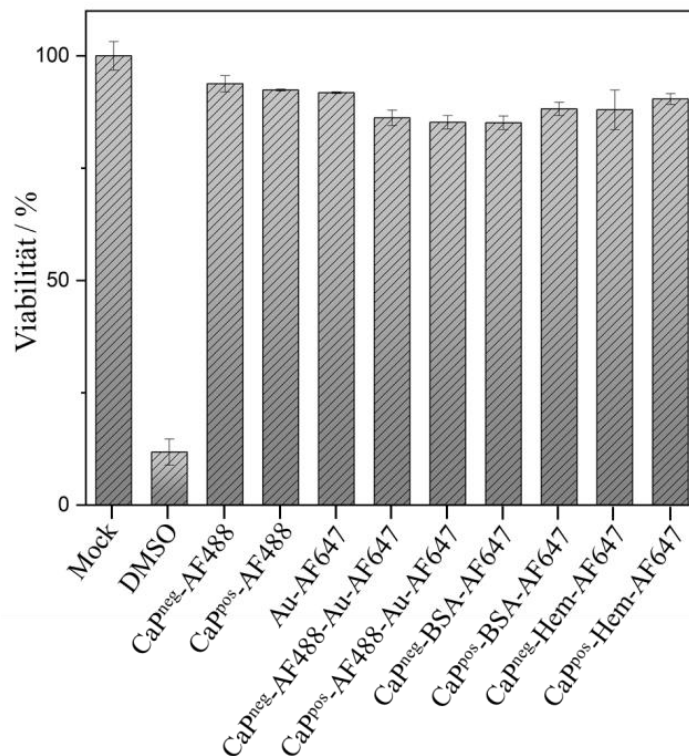


Figure 10. Viability of HeLa cells after 24 h incubation. Control groups: Mock = positive control, i.e., cells without treatment with nanoparticles. DMSO = negative control, where DMSO was added to the cells in DMEM instead of nanoparticles. The data show the average of three independent assays for each sample.

4. Conclusions

The conjugation of proteins to the surface of calcium phosphate nanoparticles via copper-catalyzed azide-alkyne cycloaddition (CuAAC, click chemistry) leads to a stable attachment. This was shown for the model proteins hemoglobin (Hem) and bovine serum albumin (BSA) and can be extended to other proteins, e.g., to antibodies or immunostimulatory proteins. To confirm the binding and to quantify the number of attached protein molecules, they were fluorescently labelled before the conjugation. Of course, this process can be skipped if functional particles shall be prepared, e.g., for therapeutic purpose. The prerequisite for CuAAC conjugation is the presence of an azide or an alkyne group on the protein. As calcium phosphate nanoparticles can be prepared with the complementary group, either one is possible. This procedure can be extended to coat large calcium phosphate nanoparticles (70 nm) with small gold nanoparticles (2 nm). There is a covalent bond between the two types of nanoparticles, again established via click chemistry. These super-particles are stable and not separated under cell culture conditions. This opens the pathway for the synthesis of multifunctional calcium phosphate particles that carry a cargo inside and functional gold nanoparticles, e.g., carrying biomolecules such as siRNA or peptides, on the outside.

The charge of the calcium phosphate nanoparticle and the cargo compounds under the moderately alkaline conditions during clicking influences the conjugation efficiency. If nanoparticle and cargo have opposite charges, the clicking is less efficient and leads to fewer clicked cargo units. Thus, a synthesis must be fine-tuned for every protein and potential cargo molecule or nanoparticle.

Finally, the fact that calcium phosphate nanoparticles were first conjugated with AF488 molecules and then with ultrasmall gold nanoparticles that attached to the remaining azide groups shows that it is possible to attach more than one species to the calcium phosphate surface. Thus, calcium phosphate nanoparticles that carry a range of species on their surface (e.g., a protein, a dye, and a gold nanoparticles) are easily conceivable. Nevertheless, their full characterization will involve careful purification, component labelling, and elemental analysis to ensure a reproducible synthesis with all cargo molecules in a defined ratio and concentration.

Author Contributions: Conceptualization, M.E.; methodology, M.E.; validation, K.K. and M.E.; formal analysis, K.K. and M.E.; investigation, K.K.; resources, M.E.; data curation, K.K. and M.E.; writing—original draft preparation, K.K.; writing—review and editing, M.E.; visualization, K.K.; supervision, M.E.; project administration, M.E. All authors have read and agreed to the published version of the manuscript.

Funding: This research received no external funding.

Data Availability Statement: Data are available from the authors upon request.

Acknowledgments: The authors thank Ursula Giebel for scanning electron microscopy and Dietrich Tönnies for X-ray powder diffraction. In addition, the authors thank the Imaging Center Campus Essen (ICCE) for access to confocal laser scanning microscopy on the Leica TCS SP8X Falcon CLSM, which was funded by the DFG (Grossgeräteprogramm nach Art. 91b GG, INST 20876/294-1 FUGG to Shirley Knauer).

Conflicts of Interest: The authors declare no conflict of interest.

References

1. Carrillo-Carrion, C.; Bocanegra, A.I.; Arnaiz, B.; Feliu, N.; Zhu, D.C.; Parak, W.J. Triple-labeling of polymer-coated quantum dots and adsorbed proteins for tracing their fate in cell cultures. *ACS Nano* **2019**, *13*, 4631–4639. [[CrossRef](#)]
2. Behzadi, S.; Serpooshan, V.; Tao, W.; Hamaly, M.A.; Alkawareek, M.Y.; Dreaden, E.C.; Brown, D.; Alkilany, A.M.; Farokhzad, O.C.; Mahmoudi, M. Cellular uptake of nanoparticles: Journey inside the cell. *Chem. Soc. Rev.* **2017**, *46*, 4218–4244. [[CrossRef](#)] [[PubMed](#)]
3. Jing, X.; Zhang, Y.; Li, M.; Zuo, X.; Fan, C.; Zheng, J. Surface engineering of colloidal nanoparticles. *Mater. Horiz.* **2023**, *10*, 1185–1209. [[CrossRef](#)]
4. Lin, Z.; Aryal, S.; Cheng, Y.H.; Gesquiere, A.J. Integration of in vitro and in vivo models to predict cellular and tissue dosimetry of nanomaterials using physiologically based pharmacokinetic modeling. *ACS Nano* **2022**, *16*, 19722–19754. [[CrossRef](#)] [[PubMed](#)]
5. Jiang, Y.; Fan, M.; Yang, Z.; Liu, X.; Xu, Z.; Liu, S.; Feng, G.; Tang, S.; Li, Z.; Zhang, Y.; et al. Recent advances in nanotechnology approaches for non-viral gene therapy. *Biomater. Sci.* **2022**, *10*, 6862–6892. [[CrossRef](#)]
6. Chung, S.; Lee, C.M.; Zhang, M. Advances in nanoparticle-based mRNA delivery for liver cancer and liver-associated infectious diseases. *Nanoscale Horiz.* **2022**, *8*, 10–28. [[CrossRef](#)] [[PubMed](#)]
7. Fleming, A.; Cursi, L.; Behan, J.A.; Yan, Y.; Xie, Z.; Adumeau, L.; Dawson, K.A. Designing functional bionanoconstructs for effective in vivo targeting. *Bioconjug. Chem.* **2022**, *33*, 429–443. [[CrossRef](#)]
8. Patel, S.; Kim, J.; Herrera, M.; Mukherjee, A.; Kabanov, A.V.; Sahay, G. Brief update on endocytosis of nanomedicines. *Adv. Drug Deliv. Rev.* **2019**, *144*, 90–111. [[CrossRef](#)]
9. Pelaz, B.; Alexiou, C.; Alvarez-Puebla, R.A.; Alves, F.; Andrews, A.M.; Ashraf, S.; Balogh, L.P.; Ballerini, L.; Bestetti, A.; Brendel, C.; et al. Diverse applications of nanomedicine. *ACS Nano* **2017**, *11*, 2313–2381. [[CrossRef](#)]
10. Tsikourkitoudi, V.; Karlsson, J.; Merkl, P.; Loh, E.; Henriques-Normark, B.; Sotiriou, G.A. Flame-made calcium phosphate nanoparticles with high drug loading for delivery of biologics. *Molecules* **2020**, *25*, 1747. [[CrossRef](#)]
11. Uskoković, V.; Tang, S.; Nikolić, M.G.; Marković, S.; Wu, V.M. Calcium phosphate nanoparticles as intrinsic inorganic antimicrobials: In search of the key particle property. *Biointerphases* **2019**, *14*, 031001. [[CrossRef](#)]
12. Degli Esposti, L.; Carella, F.; Adamiano, A.; Tampieri, A.; Iafisco, M. Calcium phosphate-based nanosystems for advanced targeted nanomedicine. *Drug Dev. Ind. Pharm.* **2018**, *44*, 1223–1238. [[CrossRef](#)]
13. Sokolova, V.; Epple, M. Biological and medical applications of calcium phosphate nanoparticles. *Chem. Eur. J.* **2021**, *27*, 7471–7488. [[CrossRef](#)] [[PubMed](#)]
14. Dorozhkin, S.V.; Epple, M. Biological and medical significance of calcium phosphates. *Angew. Chem. Int. Ed.* **2002**, *41*, 3130–3146. [[CrossRef](#)]
15. Dorozhkin, S.V. Calcium orthophosphates in nature, biology and medicine. *Materials* **2009**, *2*, 399–498. [[CrossRef](#)]

16. Kozlova, D.; Chernousova, S.; Knuschke, T.; Buer, J.; Westendorf, A.M.; Epple, M. Cell targeting by antibody-functionalized calcium phosphate nanoparticles. *J. Mater. Chem.* **2012**, *22*, 396–404. [[CrossRef](#)]
17. Rojas-Sanchez, L.; Loza, K.; Epple, M. Synthesis and intracellular tracing surface-functionalized calcium phosphate nanoparticles by super-resolution microscopy (STORM). *Materialia* **2020**, *12*, 100773. [[CrossRef](#)]
18. Rojas-Sanchez, L.; Sokolova, V.; Riebe, S.; Voskuhl, J.; Epple, M. Covalent surface functionalization of calcium phosphate nanoparticles with fluorescent dyes by copper-catalysed and by strain-promoted azide-alkyne click chemistry. *ChemNanoMat* **2019**, *5*, 436–446. [[CrossRef](#)]
19. Damm, D.; Kostka, K.; Weingärtner, C.; Wagner, J.T.; Rojas-Sanchez, L.; Gensberger-Reigl, S.; Sokolova, V.; Überla, K.; Epple, M.; Temchura, V. Covalent coupling of HIV-1 glycoprotein trimers to biodegradable calcium phosphate nanoparticles via genetically encoded aldehyde-tags. *Acta Biomater.* **2022**, *140*, 586–600. [[CrossRef](#)]
20. Kopp, M.; Kollenda, S.; Epple, M. Nanoparticle–protein interactions: Therapeutic approaches and supramolecular chemistry. *Acc. Chem. Res.* **2017**, *50*, 1383–1390. [[CrossRef](#)]
21. Wang, Y.F.; Zhou, Y.; Sun, J.; Wang, X.; Jia, Y.; Ge, K.; Yan, Y.; Dawson, K.A.; Guo, S.; Zhang, J.; et al. The Yin and Yang of the protein corona on the delivery journey of nanoparticles. *Nano Res.* **2023**, *16*, 715–734. [[CrossRef](#)] [[PubMed](#)]
22. Stauber, R.H.; Westmeier, D.; Wandrey, M.; Becker, S.; Docter, D.; Ding, G.B.; Thines, E.; Knauer, S.K.; Siemer, S. Mechanisms of nanotoxicity—Biomolecule coronas protect pathological fungi against nanoparticle-based eradication. *Nanotoxicology* **2020**, *14*, 1157–1174. [[CrossRef](#)] [[PubMed](#)]
23. McKay, C.S.; Finn, M.G. Click chemistry in complex mixtures: Bioorthogonal bioconjugation. *Chem. Biol.* **2014**, *21*, 1075–1101. [[CrossRef](#)]
24. Kolb, H.C.; Finn, M.G.; Sharpless, K.B. Click chemistry: Diverse chemical function from a few good reactions. *Angew. Chem. Int. Ed.* **2001**, *40*, 2004–2021. [[CrossRef](#)]
25. Devaraj, N.K. The future of bioorthogonal chemistry. *ACS Cent. Sci.* **2018**, *4*, 952–959. [[CrossRef](#)]
26. Qie, Y.; Yuan, H.; von Roemeling, C.A.; Chen, Y.; Liu, X.; Shih, K.D.; Knight, J.A.; Tun, H.W.; Wharen, R.E.; Jiang, W.; et al. Surface modification of nanoparticles enables selective evasion of phagocytic clearance by distinct macrophage phenotypes. *Sci. Rep.* **2016**, *6*, 26269. [[CrossRef](#)] [[PubMed](#)]
27. Yi, G.; Son, J.; Yoo, J.; Park, C.; Koo, H. Application of click chemistry in nanoparticle modification and its targeted delivery. *Biomater. Res.* **2018**, *22*, 13. [[CrossRef](#)]
28. Rueden, C.T.; Schindelin, J.; Hiner, M.C.; DeZonia, B.E.; Walter, A.E.; Arena, E.T.; Eliceiri, K.W. ImageJ2: ImageJ for the next generation of scientific image data. *BMC Bioinform.* **2017**, *18*, 529. [[CrossRef](#)]
29. Klein, K.; Loza, K.; Heggen, M.; Epple, M. An efficient method for covalent surface functionalization of ultrasmall metallic nanoparticles by surface azidation, followed by copper-catalyzed azide-alkyne cycloaddition. *ChemNanoMat* **2021**, *7*, 1330–1339. [[CrossRef](#)]
30. Meldal, M.; Tornøe, C.W. Cu-catalyzed azide–alkyne cycloaddition. *Chem. Rev.* **2008**, *108*, 2952–3015. [[CrossRef](#)]
31. Dorozhkin, S.V. Synthetic amorphous calcium phosphates (ACPs): Preparation, structure, properties, and biomedical applications. *Biomater. Sci.* **2021**, *9*, 7748–7798. [[CrossRef](#)] [[PubMed](#)]
32. Dorozhkin, S.V. Nanosized and nanocrystalline calcium orthophosphates. *Acta Biomater.* **2010**, *6*, 715–734. [[CrossRef](#)] [[PubMed](#)]
33. Urch, H.; Vallet-Regi, M.; Ruiz, L.; Gonzalez-Calbet, J.M.; Epple, M. Calcium phosphate nanoparticles with adjustable dispersability and crystallinity. *J. Mater. Chem.* **2009**, *19*, 2166–2171. [[CrossRef](#)]
34. Phan, H.T.; Bartelt-Hunt, S.; Rodenhausen, K.B.; Schubert, M.; Bartz, J.C. Investigation of bovine serum albumin (BSA) attachment onto self-assembled monolayers (SAMs) using combinatorial quartz crystal microbalance with dissipation (QCM-D) and spectroscopic ellipsometry (SE). *PLoS ONE* **2015**, *10*, e0141282. [[CrossRef](#)]
35. Luner, S.J.; Kolin, A. A new approach to isoelectric focusing and fractionation of proteins in a pH gradient. *Proc. Natl. Acad. Sci. USA* **1970**, *66*, 898–903. [[CrossRef](#)]
36. Kollenda, S.; Kopp, M.; Wens, J.; Koch, J.; Schulze, N.; Papadopoulos, C.; Pöhler, R.; Meyer, H.; Epple, M. A pH-sensitive fluorescent protein sensor to follow the pathway of calcium phosphate nanoparticles into cells. *Acta Biomater.* **2020**, *111*, 406–417. [[CrossRef](#)]
37. Rotan, O.; Severin, K.N.; Pöpsel, S.; Peetsch, A.; Merdanovic, M.; Ehrmann, M.; Epple, M. Uptake of the proteins HTRA1 and HTRA2 by cells mediated by calcium phosphate nanoparticles. *Beilstein J. Nanotechnol.* **2017**, *8*, 381–393. [[CrossRef](#)]
38. Kopp, M.; Rotan, O.; Papadopoulos, C.; Schulze, N.; Meyer, H.; Epple, M. Delivery of the autofluorescent protein R-phycoerythrin by calcium phosphate nanoparticles into four different eukaryotic cell lines (HeLa, HEK293T, MG-63, MC3T3): Highly efficient, but leading to endolysosomal proteolysis in HeLa and MC3T3 cells. *PLoS ONE* **2017**, *12*, e0178260. [[CrossRef](#)]
39. Sokolova, V.; Rotan, O.; Klesing, J.; Nalbant, P.; Buer, J.; Knuschke, T.; Westendorf, A.M.; Epple, M. Calcium phosphate nanoparticles as versatile carrier for small and large molecules across cell membranes. *J. Nanopart. Res.* **2012**, *14*, 910. [[CrossRef](#)]
40. Zarschler, K.; Rocks, L.; Licciardello, N.; Boselli, L.; Polo, E.; Garcia, K.P.; De Cola, L.; Stephan, H.; Dawson, K.A. Ultra-small inorganic nanoparticles: State-of-the-art and perspectives for biomedical applications. *Nanomedicine* **2016**, *12*, 1663–1701. [[CrossRef](#)]

41. Sokolova, V.; Kozlova, D.; Knuschke, T.; Buer, J.; Westendorf, A.M.; Epple, M. Mechanism of the uptake of cationic and anionic calcium phosphate nanoparticles by cells. *Acta Biomater.* **2013**, *9*, 7527–7535. [[CrossRef](#)] [[PubMed](#)]
42. Neuhaus, B.; Tosun, B.; Rotan, O.; Frede, A.; Westendorf, A.M.; Epple, M. Nanoparticles as transfection agents: A comprehensive study with ten different cell lines. *RSC Adv.* **2016**, *6*, 18102–18112. [[CrossRef](#)]

Disclaimer/Publisher's Note: The statements, opinions and data contained in all publications are solely those of the individual author(s) and contributor(s) and not of MDPI and/or the editor(s). MDPI and/or the editor(s) disclaim responsibility for any injury to people or property resulting from any ideas, methods, instructions or products referred to in the content.